Glial-Derived Prodegenerative Signaling in the *Drosophila* Neuromuscular System

Lani C. Keller[1], **Ling Cheng**[1], **Cody J. Locke**[1], **Martin Müller**[1], **Richard D. Fetter**[1,2], and **Graeme W. Davis**[1,*]

[1]Department of Biochemistry and Biophysics, University of California, San Francisco, 1550 4th Street, Rock Hall 4th Floor North, San Francisco, CA 94143, USA

SUMMARY

We provide evidence for a prodegenerative, glial-derived signaling framework in the *Drosophila* neuromuscular system that includes caspase and mitochondria-dependent signaling. We demonstrate that *Drosophila* TNF-α (*eiger*) is expressed in a subset of peripheral glia, and the TNF-α receptor (TNFR), Wengen, is expressed in motoneurons. NMJ degeneration caused by disruption of the spectrin/ankyrin skeleton is suppressed by an *eiger* mutation or by *eiger* knockdown within a subset of peripheral glia. Loss of *wengen* in motoneurons causes a similar suppression providing evidence for glial-derived pro-degenerative TNF-α signaling. Neither JNK nor NFκβ is required for prodegenerative signaling. However, we provide evidence for the involvement of both an initiator and effector caspase, Dronc and Dcp-1, and mitochondrial-dependent signaling. Mutations that deplete the axon and nerve terminal of mitochondria suppress degeneration as do mutations in *Drosophila* Bcl-2 (*debcl*), a mitochondria-associated protein, and Apaf-1 (*dark*), which links mitochondrial signaling with caspase activity in other systems.

INTRODUCTION

The degeneration of neuronal processes including axons, dendrites, and synaptic connections occurs during normal neuronal development and in response to neuronal injury, stress, and disease. Recent evidence in both insect dendrites (Schoen-mann et al., 2010) and mammalian neurons (Nikolaev et al., 2009) provides evidence for activation of effector caspases that can drive the destruction of neuronal processes (Nikolaev et al., 2009). An important consideration is the potential role for glia in the degenerative mechanism. Glia have been shown to engulf remnants of axons, dendrites, and nerve terminals following developmental pruning (Awasaki et al., 2006). However, it remains less clear whether glia actively participate in the degenerative signaling events that initiate and execute the pruning or degenerative process as opposed to simply cleaning up the aftermath. For example, a current hypothesis holds that degeneration during amyotrophic lateral sclerosis (ALS) may be initiated by stresses within the motoneuron and that disease progression includes a role for surrounding cell types including microglia and astrocytes (Barbeito et al., 2004; Henkel et al., 2009). However, most of the evidence supporting a role for glia in the cause or progression of ALS and motoneuron degeneration is derived from analyses at the level of the spinal cord. Very little is known about the role of peripheral glia contacting axons or the

nerve terminal. In mammals, the proinflammatory cytokine TNF-α is expressed in Schwann cells and has been implicated in the mechanisms of demyelination during multiple sclerosis (Qin et al., 2008). However, the involvement of TNF-α in ALS remains controversial. TNF-α knockout mice are viable, and elimination of TNF-α did not protect motoneurons from degeneration following overexpression of mutant SOD1 in mouse motoneurons (Gowing et al., 2006). It is worth noting that a compensatory upregulation of related proinflammatory cytokines, IL-1-β and TLR-2, was observed, and this could reasonably account for the failure of the TNF-α knockout to protect against SOD1 mediated motoneuron degeneration (Gowing et al., 2006).

We previously established a system to study motoneuron degeneration in *Drosophila*. In *Drosophila*, genetic lesions in the dynein dynactin complex (Eaton et al., 2002) and the spec-trin/ankyrin skeleton (Pielage et al., 2005, 2008, 2011; Massaro et al., 2009) disrupt axonal transport and cause degeneration of the neuromuscular junction (NMJ) and motor axons. Moto-neuron degeneration in *Drosophila* shares many of the cellular hallmarks of degeneration in mammalian neurons, observed at the light level, ultrastructurally and electrophysiologically. Genetic lesions in dynactin and the spectrin/ankyrin skeleton cause ALS and spinal cerebellar ataxia type 5 (SCA5) in humans (Puls et al., 2003; Ikeda et al., 2006). Mouse and *Drosophila* models of these diseases employing similar genetic lesions have been developed (LaMonte et al., 2002; Lorenzo et al., 2010). Taken together, these data imply that common cellular stresses are able to initiate motoneuron degeneration in insects and mammals. Furthermore, motoneuron degeneration in *Drosophila* can be suppressed by expression of a *wallerian degeneration slow* (*Wld^S*) transgene, implying the existence of common degenerative signaling pathways in mammalian and fly neuro-muscular systems (Massaro et al., 2009).

Taking advantage of an in vivo model system for motoneuron degeneration in *Drosophila*, we now provide evidence for a prodegenerative-signaling pathway that originates within the motoneuron and passages through the peripheral glia that are in close proximity to the motoneuron axon. We present evidence that TNF-α, expressed in a subset of peripheral glia, acts via a conserved TNF-α receptor (TNFR), expressed in motoneurons, to initiate prodegenerative signaling within the motor axon. The prodegenerative-signaling pathway is genetically independent of c-Jun N-terminal kinase (JNK) and NFκβ, two prominent pathways that reside downstream of the TNFR. Instead, we show that the prodegenerative process requires the *Drosophila* effector caspase, Dcp-1, which we demonstrate is both necessary and sufficient for motoneuron degeneration. Finally, we provide evidence for mitochondrial-dependent signaling in the degenerative response.

RESULTS

The development of a system to study degeneration in *Drosophila* motoneurons has allowed us to assay for mutations that are necessary for prodegenerative-signaling pathways (Eaton et al., 2002; Massaro et al., 2009; Pielage et al., 2011). We predict that loss of genes necessary for prodegenerative signaling will prevent or impair the initiation and progression of degeneration that normally occurs in animals with aberrant *spec-trin* or *ankyrin2* (*ank2*) genes. Importantly, our search for prode-generative-signaling molecules is being performed in vivo, with an intact neuromuscular system including motoneurons, muscle, and surrounding glia.

In a candidate-based screen for prodegenerative-signaling molecules, we identified a transposon insertion in the *Drosophila* homolog of TNF-α known as *eiger*. The *eiger* loss-of-function mutants have no noticeable morphological or cell death defects (Igaki et al., 2002). The transposon insertion that we identified is inserted 21 bp upstream of the

transcriptional start site and contains a GAL4 element allowing us to define the expression pattern of the *eiger* gene within the neuromuscular system (Figure 1A).

We first drove expression of *UAS-GFP* harboring a nuclear localization sequence using the *eiger*-GAL4 element. We find that *eiger*-GAL4 is expressed in a subset of glia, as identified by costaining with a pan-glial antibody (Figure 1B; also see Figure S1 available online) (anti-REPO, *Re*versed *Po*larity). Each *Drosophila* peripheral nerve contains inner glial cells that wrap the motor and sensory axons, an outer mesodermally derived perineural glial layer that does not form direct contact with axons, and third glial population termed subperineural glia that form short processes toward the axon fascicle (Stork et al., 2008). To define which subpopulation of glia expresses Eiger, we drove membrane-tethered GFP (*UAS-CD8-GFP*) using *eiger*-GAL4. We find that CD8-GFP expression surrounds the motor axons, colabeled with a marker of neuronal membranes (anti-HRP). Indeed, membrane-tethered GFP is observed to extend all the way to the site where the motor axon makes contact with muscle at the NMJ (Figure 1C). The particular site imaged at muscle 4 contains one or two motor axons surrounded by glia (Figure 1C). Consistent with recently reported data, CD8-GFP expressed in these glia rarely extends to overlap synaptic boutons within the NMJ, indicating that the glial process stops at the site of moto-neuron/muscle contact (Fuentes-Medel et al., 2009). These data indicate that *eiger* is selectively expressed in a subset of peripheral glia that surround motoneuron axons including the region of motor axons just prior to the point of nerve-muscle contact. Importantly, this is true for all peripheral NMJs that we visualized.

To investigate whether *eiger* expressing peripheral glia might be in direct contact with motor axons, we examined tangential sections of the NMJ using thin-section transmission electron microscopy (EM) (Figure 1D). We find evidence of septate junctions that are diagnostic for the interface between axons and glial cells (Banerjee and Bhat, 2008). Consistent with our light-level observations, we find evidence that peripheral glia extend all the way to the site of nerve muscle contact but do not invade the muscle cell. Instead, the glial cell ends in a foot-like structure that does not appear to include any adhesion between the glial cell and muscle membranes (Figure 1D). Thus, glia are in direct contact with the motor axon just prior to muscle invasion, and these glia are likely to be the Eiger expressing glia that we observe at the light level.

Finally, we took advantage of a previously generated anti-Eiger antibody (Igaki et al., 2009). We find that Eiger protein is enriched in peripheral nerves and that this staining is strongly diminished in a newly generated *eiger* mutation that is predicted to be a molecular null (*eiger^{A25}*; see next section) (Figures 1E–1G). Note that the images of anti-Eiger staining in peripheral nerves are projection images from confocal image stacks. Thus, the puncta of anti-Eiger that overlap neuronal anti-HRP include staining above and below the nerve bundle. We rarely observe staining within the HRP-positive nerve bundle when examining individual optical sections (data not shown). Finally, we do not observe significant Eiger staining at the NMJ, suggesting that Eiger is a glia-derived protein with a distribution that is restricted to the domain defined by the glial ensheathment of peripheral nerves.

To establish that anti-Eiger staining is derived from glia, we used a previously characterized *UAS-eiger*-RNAi transgene (Igaki et al., 2002) to knock down *eiger* expression with a neuron-specific GAL4 (*C155*-GAL4), a pan-glial GAL4 (*repo*-GAL4), or our newly identified *eiger*-GAL4 driver. Pan neuronal knockdown has no quantitative effect on the levels of Eiger staining in peripheral nerves (Figure 1G). However, both *repo*-GAL4 and *eiger*-GAL4 significantly decrease Eiger staining in peripheral nerves to levels that are not statistically significantly different from that observed in the *eiger* mutation (see Figure S2 for additional images). These data are consistent with the conclusion that Eiger protein is

derived from a subset of peripheral glia in which the *eiger* gene appears to be expressed (Figure 1).

Loss of Eiger Suppresses Neuromuscular Degeneration

We have developed a quantitative assay for neuromuscular degeneration at the *Drosophila* NMJ (Eaton et al., 2002; Eaton and Davis, 2005; Pielage et al., 2005, 2011; Massaro et al., 2009). In brief we visualize the motoneuron membrane (anti-HRP), presynaptic active zones (anti-Brp), and postsynaptic muscle folds at the NMJ (anti-Dlg). In wild-type animals there is perfect apposition of the pre- and postsynaptic markers throughout the NMJ. However, following a variety of stresses associated with the cause of neuromuscular degeneration in mammalian systems including disrupted axonal transport (Eaton et al., 2002), loss of trophic signaling (Eaton and Davis, 2005), or disruption of the spectrin/ankyrin skeleton (Pielage et al., 2005, 2011), the presynaptic terminal degenerates. The phenotype of motoneuron degeneration includes fragmentation of the presynaptic motoneuron membrane so that it is no longer continuous with the axon, altered organization of cell surface antigens including cell adhesion molecules (Pielage et al., 2005), ultrastructural evidence of degeneration based on serial EM sectioning of degenerating NMJs (Eaton et al., 2002), elimination of presynaptic antigens including anti-Brp, and morphologically disrupted mitochondria (Pielage et al., 2011). We find that loss of presynaptic antigens precedes the disassembly of the postsynaptic muscle membrane folds termed the subsynap-tic reticulum (SSR). Therefore, we can quantify sites where well-organized postsynaptic SSR is no longer opposed by the presynaptic motoneuron. We have previously demonstrated that this assay reports the degeneration of the presynaptic terminal (Eaton et al., 2002; Eaton and Davis, 2005; Pielage et al., 2005, 2011; Massaro et al., 2009), and that this degeneration is progressive during larval development (Massaro et al., 2009). This phenotype cannot be accounted for by altered synapse development or sprouting of the presynaptic nerve terminal (Eaton et al., 2002; Eaton and Davis, 2005; Pielage et al., 2005; Massaro et al., 2009).

To test a potential role for Eiger in neuromuscular degeneration, we generated a small deletion in the *eiger* gene by imprecise excision of the *eiger*-GAL4 transposon insertion, which resides 21 bp upstream of the 5′ transcriptional start site (Figure 1A). The resulting small deletion termed *eiger$^{\Delta 25}$* removes approximately 1.5 kb of genomic DNA within the *eiger* locus, starting from the site of the transposon insertion and including the predicted transcription and translational start sites as well as the entire first coding exon (Figure 1A). Therefore, the *eiger$^{\Delta 25}$* mutation is predicted to be a null mutation. Examining the NMJ of *eiger* null mutants demonstrates normal NMJ morphology and wild-type apposition of pre- and postsynaptic markers (Figure 2). Thus, *eiger* is not required for normal NMJ growth or stability.

We next asked whether loss of *eiger* could suppress NMJ degeneration in the *ank2* mutant background. As reported previously, mutations in *ank2* cause severe NMJ degeneration leading to complete elimination of the presynaptic nerve terminal at many NMJs (Figures 2C, 2E, and 2F). However, when we examine *eiger; ank2* double mutant animals, we find that the severity of NMJ degeneration is significantly suppressed (Figures 2D–2F; $p < 0.001$). To examine the tissue specificity of this effect, we knocked down Eiger in *eiger*-expressing glia using the *eiger*-GAL4 driver and demonstrate that glial-specific Eiger knockdown suppresses NMJ degeneration as efficiently as the *eiger* null mutation (Figures 2E and 2F; $p < 0.001$). These data indicate that a subset of peripheral glia is the source of Eiger that is necessary for prodegenerative signaling. The suppression of NMJ degeneration is not a secondary consequence of enhanced growth because *eiger* mutants do not have a significantly different number of boutons compared to wild-type animals (Figure S3).

We also examined other phenotypes commonly associated with neurodegeneration. The loss of *ank2* causes axonal blockages, consistent with severely disrupted axonal transport that is often associated with neuromuscular degeneration in this and other systems (LaMonte et al., 2002). Loss of *ank2* also causes a severe disruption of the axonal and synaptic microtu-bule cytoskeleton, a common stress that can lead to neuromus-cular degeneration (Bettencourt da Cruz et al., 2005). We find that both of these disease-related phenotypes are just as severe when comparing *ank2* with the *eiger; ank2* double mutant (Figure 3). These analyses include qualitative analysis of Futsch organization within the nerve terminal (Figures 3E–3H) and quantitative analysis of Brp staining within the peripheral nerves (Figures 3A–3D). Total Brp fluorescence intensity integrated over total nerve area is as follows: wt = 8.1 ± 1.0 (arbitrary fluorescence units, n = 17 nerve bundles); *eiger* = 10.5 ± 1.3 (n = 17; not significant compared to wt); *ank2* = 31.7 ± 4.5 (n = 17; p < 0.001 compared to wild-type); and *eiger; ank2* = 30.5 ± 2.9 (n = 21; p < 0.001 compared to wt and not significantly different than *ank2* alone). These data indicate that loss of Eiger does not improve neuronal health by acting directly to improve axonal transport or cytoskeletal organization. These data are also consistent with the recent demonstration that Wld^S expression can suppress NMJ degeneration in our system without affecting the presence of axonal blockages or cytoskeletal organization (Massaro et al., 2009). Together, our data demonstrate that loss of Eiger can suppress neuromuscular degeneration following a severe cytological stress to the motoneuron.

Finally, we overexpressed Eiger in peripheral glia using the *eiger*-GAL4 driver. We find no evidence of NMJ degeneration or impaired animal health (data not shown). One possibility is that Eiger overexpression is not sufficient to activate the downstream TNFR. Eiger is a type II transmembrane protein that, like TNF-α, must be cleaved in order to be secreted. In vertebrates this is achieved by TNF-α converting enzyme (TACE), and a TACE homolog is present in *Drosophila*, though no mutations in this gene currently exist.

The TNFR Wengen Functions in Motoneurons to Promote Neuromuscular Degeneration

To date, Wengen is the only known TNFR in *Drosophila* (Kanda et al., 2002; Kauppila et al., 2003). *wengen* mRNA is expressed at all stages of development, much like its ligand *eiger* (Kanda et al., 2002), and both *wengen* and *eiger* are expressed within the ventral nerve cord at late embryonic stages (Kauppila et al., 2003). It has been shown that Eiger and Wengen can interact physically with each other through their TNF homology and TNFR homology domains, respectively. This evolutionarily conserved TNF-α-like signaling pathway has now been shown to be involved in JNK-induced cell death in the fly eye (Kanda et al., 2002; Kauppila et al., 2003; Babcock et al., 2009).

We have determined that Wengen is expressed in motoneu-rons, where it could function as a receptor for glial-derived Eiger signaling. Expression of Wengen cDNA was determined by RT-PCR analysis from RNA made specifically from a FACS-sorted population of GFP-positive motoneurons isolated from third-instar larval brain (Figure S4). Because Wengen is a type I membrane protein, we tagged the C-terminal tail with a Venus tag to visualize Wengen localization (Kanda et al., 2002; Kauppila et al., 2003). When expressed in motoneurons using *OK371*-GAL4, Wengen-Venus accumulates along motor axons within peripheral nerves (Figure 4A). Wengen-Venus also traffics to the presynaptic nerve terminal at the NMJ, where it is distributed in a punctate manner throughout synaptic boutons and inter-bouton regions (Figure 4B). It is worth noting that expression in axons is considerably stronger than within the NMJ, even when one assesses staining in isolated axons just prior to muscle innervation (data not shown). Thus, the highest levels of Wengen occur in axons where it is in a position to receive signaling from glial-derived Eiger. Finally, as a control, we determined that the axonal staining does not colocalize with other synaptic protein

markers, so the accumulation of Wengen-Venus in axons cannot be attributed to impaired axonal transport (Figure S5).

In order to examine whether Wengen plays a role in neuromus-cular degeneration, we used a previously established and veri-fied *wengen* RNAi (*wgn*RNAi) construct (Kanda et al., 2002; Kauppila et al., 2003; Babcock et al., 2009; Xue et al., 2007; Igaki et al., 2002) in an attempt to suppress the degeneration phenotype observed in *ank2* mutants. Animals with knockdown of *wengen* in motoneurons show no evidence of NMJ degeneration (Figures 4C, 4E, and 4F). However, neuronal expression of *wgn*RNAi in an *ank2* background significantly suppresses the severity of synaptic degeneration when compared with *ank2* animals alone (Figures 4D–4F). Again, this suppression of neuro-muscular degeneration cannot be accounted for by enhanced synaptic growth because bouton numbers are normal when *wgn*RNAi is neuronally expressed in an otherwise wild-type background (Figure S3). Again, we controlled for the presence of axonal blockages and defects in synaptic microtubules following *wgn*RNAi in the *ank2* mutant background. There is no suppression of axonal blockages nor is there an improvement in the organization of the microtubule cytoskeleton (Figure S6). Thus, Wengen is expressed in motoneurons, traffics to the axon and presynaptic nerve terminal, and is necessary, in moto-neurons, for efficient neuromuscular degeneration following a cellular stress. These data are consistent with Wengen being a receptor for glial-derived Eiger in a prodegenerative-signaling pathway. Finally, we find that Wengen overexpression is not sufficient to cause NMJ degeneration and does not alter animal health (data not shown). These data indicate that receptor over-expression is not sufficient to activate this signaling pathway in vivo.

Loss of Eiger or Wengen in the ank2 Mutant Background Improves Neuromuscular Function

We first demonstrate that *eiger* mutants have average EPSP amplitudes that are statistically similar to wild-type (Figure 5B). Next, we confirmed that the loss of *ank2* results in impaired average EPSP amplitudes (average EPSP = 29.5mV; Figure 5B). The occurrence of severely degenerated NMJs in *ank2* mutants (Figures 2E and 2F) correlates well with the number of recordings that show large defects in EPSP amplitude compared to wild-type (Figure 5; Pielage et al., 2005). Next, we demonstrate that animals homozygous for both *eiger* and *ank2* exhibit a significant recovery in synaptic neurotransmission (from 29.5mV in *ank2* mutants to 35.9 mV in *eiger; ank2* double mutants) and a near complete rescue in the number of small EPSPs (below 25 mV; Figure 5B). There is no consistent change in mEPSP amplitude that could account for these changes in EPSP amplitude (Figure 5A). Together, these results demonstrate that loss of Eiger can significantly improve the physiological function of the *ank2* mutant NMJs, consistent with a functional improvement at the NMJ that parallels suppression of anatomical degeneration.

It should be noted that average EPSP amplitude is not completely restored to wild-type values despite the general improvement of synaptic function described above. This is likely because we have not rescued all aspects of neuronal health. As show in Figure 3, there remain defects in axonal transport and microtubule organization that could reasonably impair synaptic transmission. Thus, although we have restored anatomical and functional stability, we have not completely restored neuronal health.

Finally, we also recorded from *ank2* mutants in which *wgn*RNAi is expressed presynaptically (Figure 5). In this case there is improved synaptic transmission that is similar to that observed in the *eiger; ank2* double mutant (Figure 5D; p = 0.05). These data demonstrate that the loss of *wengen* in neurons causes a functional improvement at the NMJ of the *ank2* mutant, consistent with what is observed in the *eiger; ank2* double mutant.

The Effector Caspase Dcp-1 Is Necessary and Sufficient for Neuromuscular Degeneration without Cell Death in the ank2 Mutant

Previously, it was proposed that Wengen does not possess a Death Domain that is generally thought to be necessary for activation of caspase signaling (Kanda et al., 2002). We now provide evidence for the existence of a Death Domain in Wengen based on a more extensive sequence analysis comparing residues critical for caspase-mediated signaling (McDonald et al., 2001; Figure S7). This analysis supports the possibility that Wengen could signal directly to axonal and synaptic caspases.

There are seven caspases encoded in the *Drosophila* genome including the initiator caspases Dredd, Nc (Dronc), and Strica, and the effector caspases Drice, Dcp-1, Decay, and Damm. Of the effector caspases only Drice and Dcp-1 have been shown to be enriched in the larval nervous system, whereas Dronc and Dredd are initiator caspases with enriched expression in the larval CNS (Chintapalli et al., 2007). We first tested whether caspase overexpression might cause motoneuron degeneration. Overexpression of the initiator caspase Dredd in motoneu-rons was without effect. However, overexpression of Dronc in motoneurons caused embryonic lethality, suggesting that Dronc might be an initiator caspase in motoneurons. We then decreased GAL4-dependent *UAS-Dronc* expression by lowering the temperature at which we raised the animals to 18°C. Under this condition, rare larvae survive to late larval stages (Figure 6F). These animals show severe NMJ degeneration with many complete NMJ eliminations. These data demonstrate that Dronc expression is sufficient to cause NMJ degeneration. Consistent with this finding, we demonstrate that Flag-tagged Dronc (Yang et al., 2010) traffics to the axon and presynaptic nerve terminal (Figure 7A).

We next overexpressed effector caspases. Drice was without effect. By contrast, overexpression of *UAS-Dcp-1* in motoneu-rons caused severe motoneuron degeneration (Figure 6). We confirmed the severity of anatomical NMJ degeneration by recording from these NMJs. We demonstrate that synaptic transmission is severely disrupted (Figure S8). Next, we coex-pressed *UAS-Dcp-1* and *UAS-CD8-GFP* in a small subset of motor axons using the *Eve*-GAL4 driver so that we could visualize individual axons in the peripheral motor nerve. We label between one and four motor axons with *UAS-CD8-GFP* using the *Eve*-GAL4 driver. Overexpression of *UAS-CD8-GFP* alone labels individual motor axons that can be traced continuously, without break, from the CNS to the NMJ (Figure 6C). By contrast, when *UAS-CD8-GFP* is coexpressed with *UAS-Dcp-1*, we find clear evidence that axons have a narrower caliber and clear evidence of axonal breaks or fragmentation (Figure 6D). These data demonstrate that expression of *UAS-Dcp-1* causes axonal degeneration as well as degeneration at the nerve terminal. As a control, we demonstrate that the glial expression of *UAS-Dcp-1* is without effect (Figure 6E). As with the initiator caspase Dronc, Venus-tagged Dcp-1 traffics to the axon and presynaptic nerve terminal (Figure 7B).

The observation that overexpression of *UAS-Dcp-1* is able to initiate caspase activity suggests that this caspase can be autoactivated through overexpression because it seems unlikely that there is a constitutively active initiator caspase activity in motoneurons. This is consistent with prior demonstration that caspase 6, unlike caspase 3 and 7, can undergo autoactivation (Klaiman et al., 2009; Wang et al., 2010). At present, we cannot rule out the possibility that Drice is ineffective at causing NMJ degeneration because it requires initiator caspase activity in motoneurons.

There are two additional features of this experiment that are interesting. First, axonal degeneration following expression of *UAS-Dcp-1* does not spread to adjacent axons in this system. When *UAS-Dcp-1* is expressed by *Eve*-GAL4, only one of two motor axons is labeled that innervate muscle 1. We find evidence of degeneration at the motoneuron

expressing *UAS-Dcp-1*, but not in the adjacent axon innervating the same muscle target (there is also no evidence of compensatory growth of the remaining terminal) (data not shown). Second, we find no evidence of neuronal sprouting at sites of broken axons. We presume that this is due to the fact that these axons are undergoing active degeneration and are not responding to injury or physical breakage, which can lead to sprouting (Ayaz et al., 2008). Finally, degeneration following expression of *UAS-Dcp-1* does not include motoneuron cell death. We assayed cell death using a TUNEL assay and found no evidence of motoneuron cell death (data not shown), consistent with prior evidence of NMJ degeneration without cell death in the *ank2* mutation (Pielage et al., 2008), following loss of spectrin (Pielage et al., 2005) and following disruption of axonal transport (Eaton et al., 2002). This is also consistent with caspase 6 activation not causing cell death in mammalian systems (Klaiman et al., 2009; Nikolaev et al., 2009).

Because overexpression of *UAS-Dcp-1* is sufficient to cause motoneuron degeneration, we asked whether loss of Dcp-1 could suppress NMJ degeneration in the *ank2* mutant background. We acquired a strong loss-of-function mutation in *Dcp-1* (Laundrie et al., 2003) and generated double mutant combinations with *ank2*. We find that loss of Dcp-1 alone does not have any significant effect on larval viability or NMJ integrity or growth (Figure S3). Remarkably, we find that NMJ degeneration is almost completely blocked in the *dcp-1; ank2* double mutant (Figures 6G and 6H; see also Figure S9 for representative images of suppression). Even more remarkable, a heterozygous *dcp-1/+* mutation is nearly as effective at blocking neuromus-cular degeneration (Figures 6G and 6H), indicating that the degenerative response is strikingly sensitive to the levels of Dcp-1. Thus, our data demonstrate that Dcp-1 is both necessary for degeneration following a cytological stress and is sufficient to drive neuromuscular and axonal degeneration.

Finally, because Eiger appears to be absent from the NMJ where degeneration occurs, we asked whether the caspases might be mobile within the neuron and thereby capable of causing degeneration at sites distant from signal initiation. We used Dcp-1-Venus, which will tag both active and inactive Dcp-1 protein, and performed standard FRAP (fluorescence recovery after photobleaching) analysis. We find that a significant fraction of Dcp-1-Venus is diffusible within the axon (Figures 7C–7E). This is consistent with the possibility that caspases could cause destruction at a distance from the site of activation. However, we acknowledge that other signaling components could also be mobile and causal.

Evidence for Localized, Mitochondria-Dependent, Prodegenerative Signaling

We next explored other potential components of Eiger-Wengen prodegenerative signaling. Three prominent signaling pathways have been defined downstream of TNFRs in other systems that can be distinguished by the involvement of NFκβ, JNK, and caspases (Aggarwal, 2000). In the *Drosophila* visual system, Eiger and Wengen have been shown to influence JNK signaling (Kauppila et al., 2003). However, rather than suppressing degeneration, we find that NMJ degeneration is moderately enhanced by expression of *dnJNK*, perhaps consistent with a function for JNK in axonal transport (Figure 8A). Next, we tested whether a null mutation in the *Drosophila* homolog of NFκβ (*dorsal*) suppresses NMJ degeneration. We previously demonstrated that the presynaptic nerve terminal in *dorsal* mutants is anatomically normal (Heckscher et al., 2007). Here, we show that the *dorsal* mutation does not suppress NMJ degeneration in the *ank2* mutant (Figure 8B). These data rule out two prominent downstream signaling systems linked to TNFR signaling, further supporting the possibility that Wengen may signal primarily to downstream caspases including Dcp-1.

Mitochondria are also integrally involved in proapoptotic signaling pathways (Wang and Youle, 2009). However, a role for mitochondria in developmental pruning and local

degeneration without cell death remains virtually unknown. In *Drosophila* the *miro* mutation allows us to test whether axonal and synaptic mitochondria are necessary for the progression of prodegenera-tive signaling in the periphery. In *miro* mutants the majority of mitochondria remain stranded in the neuronal soma and soma-proximal axon, whereas the distal axon and presynaptic nerve terminal are largely devoid of this organelle. This was confirmed by MitoTracker staining (Figure S10). Remarkably, the larval nervous system is fully functional, and synaptic transmission remains robust in the *miro* mutant (Guo et al., 2005; Russo et al., 2009).

First, we examined synapse morphology in *miro* mutants and found no evidence of NMJ degeneration or altered neuromuscular growth (Figure S3). We then examined *miro* mutations in animals also expressing a presynaptic *α-spectrin*-RNAi construct that alone shows significant degeneration (Figures 8C and 8D). Remarkably, the presence of the *miro* mutation caused a dramatic suppression of neuromuscular degeneration (Figures 8C and 8D). We confirmed that mitochondria are diminished in axons of the *α-spectrin*-RNAi; *miro* double mutant, just as in *miro* mutants alone (Figure S10). Because mitochondria are decreased in number in the distal motoneuron axon and in the synapse, these data suggest that that there could be a localized function for mito-chondria in the axon and/or presynaptic nerve terminal that participates in prodegenerative signaling.

It remains a formal possibility that the Miro molecule itself is essential for prodegenerative signaling. To further investigate the role of mitochondria-dependent signaling in axonal and synapse degeneration, we examined mutations in two additional genes previously linked to mitochondrial-dependent signaling that drives or potentiates caspase activity in other systems (Wang and Youle, 2009). First, we demonstrate that a loss-of-function mutation in the *Drosophila* death executioner Bcl-2 homolog, *debcl* (Sevrioukov et al., 2007) alone does not cause NMJ degeneration or changes in NMJ morphology (Figures 8E and 8F; Figure S3). However, when *debcl* is placed in the *ank2* mutant background, degeneration is statistically significantly suppressed (Figures 8E and 8F). It is well established that Debcl directly associates with mito-chondria in *Drosophila* and other systems and promotes cas-pase activity following mitochondrial disruption (Doumanis et al., 2007). Next, we performed an identical analysis with the *Drosophila* Apaf-1 (Apoptotic protease activating factor 1) homolog termed Dark. Dark is known to act in a signaling system downstream of mitochondrial disruption and is important for the activation of the initiator caspase Dronc (reviewed in Richardson and Kumar, 2002). Importantly, previous genetic work has shown that *dark* interacts genetically with both *dronc* and *dcp-1* (Richardson and Kumar, 2002), the precise cas-pases that we implicate in *ank2*-dependent NMJ degeneration (see above). Here, we show that a loss-of-function *dark* mutation has no effect on NMJ morphology (Figure S3), but *dark* significantly suppresses *ank2*-dependent NMJ degeneration (Figures 8G and 8H). When taken in context with previously published genetic interactions, our data are consistent with an emerging signaling system that couples disruption of mito-chondria to Debcl, Dark, and downstream caspase activity. We note that the suppression of NMJ degeneration by *debcl* and *dark* is not as dramatic as suppression by *dcp-1* mutations. This is consistent with current models in which mitochon-drial-dependent signaling, via these proteins, functions to potentiate caspase activity that has been stimulated through other events including proinflammatory cytokine signaling (Richardson and Kumar, 2002; Wang and Youle, 2009). As such, loss of these proteins may suppress amplification of caspase activity but not block caspase activity. Finally, again consistent, there is recently published evidence that disruption of the spectrin/ankyrin/adducin skeleton causes a disruption of mitochondria that resembles, phenotypically, mitochondrial disruptions observed in diverse models of neurodegenerative disease (Pielage et al., 2011; Menzies et al., 2002).

DISCUSSION

Here, we provide evidence for a prodegenerative-signaling system that originates in motoneurons following a cellular stress, passages through peripheral glial cells that are in close proximity to the motoneuron axons, and ultimately includes the activation of an effector caspase in the motoneuron that drives local degeneration (Figure 9). These data also raise important questions. We do not know how motoneuron stress is signaled to the surrounding glia. One possibility is that this involves a factor released from the motoneuron and detected by a receptor on the glial cell. An alternative is that the glial cell could sense a physical stress such as axonal swelling that has been shown to accompany axonal blockages following disruption of axonal transport and disruption of the spectrin/ankyrin skeleton (Pilling et al., 2006; Shah et al., 2009). We have yet to devise a constitutively active Wengen receptor. As such, we are unable to provide formal evidence that loss of Dcp-1 is able to suppress prodegenerative signaling from the Wengen receptor. However, the near-complete suppression of neurodegeneration by the loss of Dcp-1 and the observation that Dcp-1 is sufficient to cause profound degeneration support the idea that Dcp-1 is the final stage in the degenerative signaling cascade and likely functions downstream of Wengen. Finally, we have yet to establish precisely where mitochondria-dependent signaling fits into the prodegenerative cascade, and we discuss different possibilities in greater detail below.

Glial Signaling in Motoneuron Degenerative Disease

Current models of neurodegenerative signaling in the neuromus-cular system suggest that degeneration is initiated by cellular stress in the motoneuron and that glial cells (microglia or astro-cytes) participate in the progression of degenerative disease. The participation of microglia and astrocytes occurs primarily within the spinal cord, not within peripheral axons, and is thought to contribute to the spread of degeneration throughout the moto-neuron pool (Barbeito et al., 2004). Our data imply that peripheral glia cells could be directly involved in the prodegenerative pathway by secreting TNF-α. It may be reasonable to suspect parallel signaling in mammalian systems. TNF-α is expressed by Schwann cells, and TNF-α signaling from Schwann cells has been implicated in proinflammatory disease including multiple sclerosis (Qin et al., 2008).

A role for TNF-α in motoneuron degenerative disease such as ALS was largely discounted a number of years ago when it was demonstrated that expression of mutant SOD1 in motoneurons of TNF-α knockout mice resulted in motoneuron degeneration that was no different than that observed in a wild-type background (Gowing et al., 2006). However, several issues are worth considering. First, SOD1 transgenes were highly expressed, far beyond that that is observed in disease, and this may have overcome any protective effect provided by the absence of TNF-α. Second, even in *Drosophila*, loss of TNF-α provides a modest protective effect compared to loss of the effector caspase Dcp-1. Third, it was demonstrated that two other TNF-α-like cytokines are upregulated in the TNF-α knockout mouse, indicating a possible compensatory process. It might be reasonable, given the many examples of compensatory regulation within signaling systems of knockout mice, to suspect that the upregu-lated cytokines replaced TNF-α signaling functions during prode-generative signaling in these experiments.

What might be the logic for incorporating a glial cell in the induction of prodegenerative signaling? A likely explanation is that by partitioning the prodegenerative-signaling system between two cells, additional layers of control can be imposed on the system so that errant activation of degeneration is unlikely. For example TNF-α activating enzyme (TACE) is required to cleave TNF-α prior to secretion and represents an essential form of regulation that may be required in glia. In addition full activation of the degenerative response might include active insertion of the TNFR in the membrane by the moto-neuron. This

organization would restrict the spread of prodege-nerative signaling such that only motoneurons that have been stressed and have actively inserted TNFR in the membrane will respond to TNF-α released from the glial cell and degenerate. This possibility remains to be tested.

Localization and Control of Prodegenerative Signaling

Here, we demonstrate that peripheral glial cells that surround motor axons express Eiger. Because Eiger knockdown in these cells is sufficient to suppress degeneration after an axonal insult, we conclude that Eiger has the potential to activate prodegener-ative signaling via the Wengen receptor along the length of the motor axons, as diagrammed in Figure 9. However, it remains unknown how this prodegenerative signaling spreads to drive the degeneration of the presynaptic nerve terminal at the NMJ because glial ensheathment of motor axons stops prior to the NMJ (Figure 1). One possibility is that dynamic invasion of the NMJ by peripheral glia conveys prodegenerative signaling to this site (Fuentes-Medel et al., 2009). Another possibility is that caspases, once activated in the axon, can be mobilized to the presynaptic terminal of the NMJ. This possibility is consistent with the catalytic activity of caspases and our demonstration of caspase mobility within motor axons (Figure 7C). Ultimately, the mechanisms that disseminate prodegenerative signaling throughout a cell are not well understood. Likewise, it is not understood how prodegenerative signaling responsible for selective dendrite pruning is restricted to specific neuronal compartments. Finally, it is worth emphasizing that many of the prodegenerative-signaling molecules identified in our study do not adversely effect neuromuscular development when mutated or deleted. For example mutations in *eiger*, *dcp-1*, *debcl*, and *dark* show no obvious NMJ phenotype in larval stages and are homozygous viable as adult flies. Thus, the neuroprotec-tive effects of these loss-of-function mutations can be separated from the molecular mechanisms of motoneuron growth control. As such, these proteins could be considered good potential targets for therapeutic intervention aimed at slowing the progression of neuromuscular degeneration.

Mitochondrial Signaling during Neurodegenerative Disease

Our data provide evidence that mitochondria are required in the local axon and synaptic environments during prodegenerative signaling. In addition we recently established that mitochondria are disrupted, visualized ultrastructurally, in nerve terminals undergoing degeneration (Pielage et al., 2011), consistent with findings in mammalian systems and human disease (Menzies et al., 2002; Martin et al., 2007). In our experiments, the *miro* mutation causes depletion of mitochondria from the axon and nerve terminal, stranding them primarily in the motoneuron soma and proximal axons. Yet, in the *miro* mutant background, α-spectrin-dependent degeneration is suppressed. This finding is in apparent contrast to the well-established function for mito-chondria in the cell body during proapoptotic cell death signaling cascades (reviewed in Wang and Youle, 2009). Although proapoptotic signaling from mitochondria is strongly implicated in neurodegenerative disease, our data suggest that mitochon-dria might represent a means to restrict or locally modulate prodegenerative signaling within specific neuronal compartments, based on data from the *miro* mutant background (Figure 8D).

In *Drosophila,* the Bcl-2 homolog Debcl functions to promote mitochondrial cytochrome *c* release that, in turn, modulates Dark-dependent activation of the initiator caspase Dronc (Richardson and Kumar, 2002). Active Dronc mediates the activation of effector caspases including Dcp-1. By demonstrating that mutations in both *debcl* and *dark* suppress neurodegenera-tion, we provide evidence that signaling downstream of mito-chondria interfaces with the degenerative signaling pathway, potentially serving to amplify caspase activity. This is consistent with previously published data showing that mutations of two

other proapoptotic Bcl-2 family proteins in a mouse model of familial ALS not only halt neuronal loss but also prevent axonal degeneration and paralysis (Reyes et al., 2010).

EXPERIMENTAL PROCEDURES

Fly Stocks

Flies were maintained at 25°C on normal food, unless otherwise noted. The following strains were used in this study: w^{1118} (wild-type); $egr^{\Delta25}$ (generation of mutants described below); $elav^{C155}$-GAL4 (neuron-specific; Lin and Goodman, [1994]); $OK371$-GAL4 (motoneuron-specific; Bloomington Stock Center, Bloomington, IN, USA); $eveRRa$-GAL4 (courtesy of R. Baines, University of Manchester); egr-GAL4 (courtesy of Heberlein Lab, UCSF; position of insertion was verified by standard reverse PCR); $repo$-GAL4 (Bloomington Stock Center); $ank2^{2001}$ (Pielage et al., 2008); dcp-1^{Prev1} (courtesy of K. McCall, Boston University; Laundrie et al., [2003]); $pUAS$-Dcp-1, $pUAS$-$Drice$, $pUAS$-$Dredd$, $pUAS$-$Dronc$ (courtesy of O. Yoo, Korea Advanced Institute of Science and Technology); $pUAS$-$wengen$-RNAi (courtesy of M. Miura, RIKEN Brain Science Institute); UAS-$DNbsk$ (Weber et al., 2000); UAS-α-$spectrin$-RNAi (line 110417; Vienna *Drosophila* RNAi Center); $miro^{B682}$ (courtesy of K.E. Zinsmaier, University of Arizona); UAS-$CD8$-GFP, UAS-$nuclear$-$localization$-$signal$-GFP, $pUAS$-egr-$RNAi$ (courtesy of M. Miura); $pUAS$-$Dronc$-FLAG (courtesy of S. Kornbluth); $dark^{CD4}$ (courtesy of J.M. Abrams); $debcl$ [E26] (Bloomington Stock Center); and dl^1 (Bloomington Stock Center).

Generation of Wgn-Venus and Dcp-1-Venus Flies

The full-length Wengen cDNA RE29502 and the full-length Dcp-1 cDNA LD13945 were obtained from the Drosophila Genomics Research Center (Indiana University, Bloomington, IN, USA) and tagged with a C-terminal fusion protein encoding the fluorescent protein Venus by cloning into the plasmid PtWV using the Gateway System (Carnegie *Drosophila* Gateway Collection). Transgenic flies were produced and balanced using standard procedures (BestGene).

Generation of eiger Null Mutants

Excision lines of *eiger* were generated by the excision of the transposon insertion line *egr-GAL4* using the *delta[2–3]* transposase. PCR screening with homozygous progeny was performed with primers 5′-gcaggcgcccttaagtatg-3′ and 5′-gcttgatcagccaagaaacc-3′. Sequencing of PCR products revealed that ~1.5 kb of the genomic region was deleted in $egr^{\Delta25}$.

Immunohistochemistry

Wandering third-instar larvae were dissected and stained according to standard procedures (Massaro et al., 2009). Primary antibodies were used at the following dilutions: 1:100 anti-Bruchpilot (Developmental Studies Hybridoma Bank); 1:20 anti-Futsch (22C10; Developmental Studies Hybridoma Bank); 1:10,000 anti-Dlg (anti-Discs large); 1:500 anti-Eiger (courtesy of M. Miura); 1:400 anti-GFP (3E6; Invitrogen); and 1:20 anti-Repo (BD12; Developmental Studies Hybridoma Bank). Secondary Alexa Fluor antibodies (goat anti-mouse 488, goat anti-rabbit 555, and goat anti-rabbit 647) were obtained from Invitro-gen and diluted in PBT to a final concentration of 1:500. All other secondary antibodies and Cy3- and Cy5-conjugated HRP were obtained from Jackson ImmunoResearch Laboratories, Inc., or Invitrogen and used at a 1:300 dilution.

Imaging and Analysis

Images were digitally captured using a CoolSNAPHQ CCD camera mounted on a Zeiss Axiovert 200 M microscope and analyzed using SlideBook software (Intelligent Imaging Innovations). Individual nerves and synapses were optically sectioned at 0.5 μm using a piezoelectric-driven z-drive controlling the position of a Zeiss Plan-Apochromat 100× oil immersion objective (NA = 1.4). Images were deconvolved with the nearest neighbor algorithm, and Z stacks were combined into a single projection image. For quantification of Brp fluorescence within nerves, the maximum fluorescence intensity of each Brp punctum within a nerve area was determined for each 2D projection image using a semiautomated procedure as described previously (Massaro et al., 2009; Heckscher et al., 2007). Image stacks were taken at the same exposure from animals projected into a single 3D stack before masking. No alterations were made to the images before quantification.

NMJ Degeneration Quantification

Degeneration was scored at 40× magnification with the observer being blind to the genotype. Segments A2–A6 were counted, and a degenerative event was defined as an area of the NMJ with clearly defined postsynaptic Dlg staining without any apposing presynaptic Brp staining.

EM

Wild-type third-instar larvae were prepared for EM as described (Pielage et al., 2011).

Electrophysiology

Recordings were made in HL3 saline (Ca^{2+} 0.4 mM, Mg^{2+} 10 mM) from muscle 6 in abdominal segment 3 of third-instar larvae as previously described (Massaro et al., 2009). Measurements of EPSP and spontaneous miniature release event amplitudes were made using semiautomated routines in Mini Analysis software (Synapsoft). Recordings were accepted for measurement with resting potentials more hyperpolarized than −60 mV and with input resistances greater than 5 MΩ.

FRAP

FRAP experiments were performed within single axons projecting to muscle 4 (segments A2 and A3) of wandering third-instar larvae. See Supplemental Experimental Procedures.

Supplementary Material

Refer to Web version on PubMed Central for supplementary material.

Acknowledgments

References

Aggarwal BB. Tumour necrosis factors receptor associated signalling molecules and their role in activation of apoptosis, JNK and NF-kappaB. Ann Rheum Dis. 2000; 59(Suppl 1):i6–i16. [PubMed: 11053079]

Awasaki T, Tatsumi R, Takahashi K, Arai K, Nakanishi Y, Ueda R, Ito K. Essential role of the apoptotic cell engulfment genes draper and ced-6 in programmed axon pruning during *Drosophila* metamorphosis. Neuron. 2006; 50:855–867. [PubMed: 16772168]

Ayaz D, Leyssen M, Koch M, Yan J, Srahna M, Sheeba V, Fogle KJ, Holmes TC, Hassan BA. Axonal injury and regeneration in the adult brain of *Drosophila*. J Neurosci. 2008; 28:6010–6021. [PubMed: 18524906]

Babcock DT, Landry C, Galko MJ. Cytokine signaling mediates UV-induced nociceptive sensitization in *Drosophila* larvae. Curr Biol. 2009; 19:799–806. [PubMed: 19375319]

Banerjee S, Bhat MA. Glial ensheathment of peripheral axons in *Drosophila*. J Neurosci Res. 2008; 86:1189–1198. [PubMed: 18041093]

Barbeito LH, Pehar M, Cassina P, Vargas MR, Peluffo H, Viera L, Estévez AG, Beckman JS. A role for astrocytes in motor neuron loss in amyotrophic lateral sclerosis. Brain Res Brain Res Rev. 2004; 47:263–274. [PubMed: 15572176]

Bettencourt da Cruz A, Schwärzel M, Schulze S, Niyyati M, Heisenberg M, Kretzschmar D. Disruption of the MAP1B-related protein FUTSCH leads to changes in the neuronal cytoskeleton, axonal transport defects, and progressive neurodegeneration in *Drosophila*. Mol Biol Cell. 2005; 16:2433–2442. [PubMed: 15772149]

Chintapalli VR, Wang J, Dow JA. Using FlyAtlas to identify better *Drosophila melanogaster* models of human disease. Nat Genet. 2007; 39:715–720. [PubMed: 17534367]

Doumanis J, Dorstyn L, Kumar S. Molecular determinants of the subcellular localization of the *Drosophila* Bcl-2 homologues DEBCL and BUFFY. Cell Death Differ. 2007; 14:907–915. [PubMed: 17205077]

Eaton BA, Davis GW. LIM Kinase1 controls synaptic stability downstream of the type II BMP receptor. Neuron. 2005; 47:695–708. [PubMed: 16129399]

Eaton BA, Fetter RD, Davis GW. Dynactin is necessary for synapse stabilization. Neuron. 2002; 34:729–741. [PubMed: 12062020]

Fuentes-Medel Y, Logan MA, Ashley J, Ataman B, Budnik V, Freeman MR. Glia and muscle sculpt neuromuscular arbors by en-gulfing destabilized synaptic boutons and shed presynaptic debris. PLoS Biol. 2009; 7:e1000184. [PubMed: 19707574]

Gowing G, Dequen F, Soucy G, Julien JP. Absence of tumor necrosis factor-alpha does not affect motor neuron disease caused by super-oxide dismutase 1 mutations. J Neurosci. 2006; 26:11397–11402. [PubMed: 17079668]

Guo X, Macleod GT, Wellington A, Hu F, Panchumarthi S, Schoenfield M, Marin L, Charlton MP, Atwood HL, Zinsmaier KE. The GTPase dMiro is required for axonal transport of mitochondria to *Drosophila* synapses. Neuron. 2005; 47:379–393. [PubMed: 16055062]

Heckscher ES, Fetter RD, Marek KW, Albin SD, Davis GW. NF-kappaB, IkappaB, and IRAK control glutamate receptor density at the *Drosophila* NMJ. Neuron. 2007; 55:859–873. [PubMed: 17880891]

Henkel JS, Beers DR, Zhao W, Appel SH. Microglia in ALS: the good, the bad, and the resting. J Neuroimmune Pharmacol. 2009; 4:389–398. [PubMed: 19731042]

Igaki T, Kanda H, Yamamoto-Goto Y, Kanuka H, Kuranaga E, Aigaki T, Miura M. Eiger, a TNF superfamily ligand that triggers the *Drosophila* JNK pathway. EMBO J. 2002; 21:3009–3018. [PubMed: 12065414]

Igaki T, Pastor-Pareja JC, Aonuma H, Miura M, Xu T. Intrinsic tumor suppression and epithelial maintenance by endocytic activation of Eiger/TNF signaling in *Drosophila*. Dev Cell. 2009; 16:458–465. [PubMed: 19289090]

Ikeda Y, Dick KA, Weatherspoon MR, Gincel D, Armbrust KR, Dalton JC, Stevanin G, Dürr A, Zühlke C, Bürk K, et al. Spectrin mutations cause spinocerebellar ataxia type 5. Nat Genet. 2006; 38:184–190. [PubMed: 16429157]

Kanda H, Igaki T, Kanuka H, Yagi T, Miura M. Wengen, a member of the *Drosophila* tumor necrosis factor receptor superfamily, is required for Eiger signaling. J Biol Chem. 2002; 277:28372–28375. [PubMed: 12084706]

Kauppila S, Maaty WS, Chen P, Tomar RS, Eby MT, Chapo J, Chew S, Rathore N, Zachariah S, Sinha SK, et al. Eiger and its receptor, Wengen, comprise a TNF-like system in *Drosophila*. Oncogene. 2003; 22:4860–4867. [PubMed: 12894227]

Klaiman G, Champagne N, LeBlanc AC. Self-activation of Caspase-6 in vitro and in vivo: Caspase-6 activation does not induce cell death in HEK293T cells. Biochim Biophys Acta. 2009; 1793:592–601. [PubMed: 19133298]

LaMonte BH, Wallace KE, Holloway BA, Shelly SS, Ascaño J, Tokito M, Van Winkle T, Howland DS, Holzbaur EL. Disruption of dynein/dynactin inhibits axonal transport in motor neurons causing late-onset progressive degeneration. Neuron. 2002; 34:715–727. [PubMed: 12062019]

Laundrie B, Peterson JS, Baum JS, Chang JC, Fileppo D, Thompson SR, McCall K. Germline cell death is inhibited by P-element insertions disrupting the dcp-1/pita nested gene pair in *Drosophila*. Genetics. 2003; 165:1881–1888. [PubMed: 14704173]

Lin DM, Goodman CS. Ectopic and increased expression of Fasciclin II alters motoneuron growth cone guidance. Neuron. 1994; 13:507–523. [PubMed: 7917288]

Lorenzo DN, Li MG, Mische SE, Armbrust KR, Ranum LP, Hays TS. Spectrin mutations that cause spinocerebellar ataxia type 5 impair axonal transport and induce neurodegeneration in *Drosophila*. J Cell Biol. 2010; 189:143–158. [PubMed: 20368622]

Martin LJ, Liu Z, Chen K, Price AC, Pan Y, Swaby JA, Golden WC. Motor neuron degeneration in amyotrophic lateral sclerosis mutant superoxide dismutase-1 transgenic mice: mechanisms of mitochon-driopathy and cell death. J Comp Neurol. 2007; 500:20–46. [PubMed: 17099894]

Massaro CM, Pielage J, Davis GW. Molecular mechanisms that enhance synapse stability despite persistent disruption of the spectrin/an-kyrin/microtubule cytoskeleton. J Cell Biol. 2009; 187:101–117. [PubMed: 19805631]

McDonald ER 3rd, Chui PC, Martelli PF, Dicker DT, El-Deiry WS. Death domain mutagenesis of KILLER/DR5 reveals residues critical for apoptotic signaling. J Biol Chem. 2001; 276:14939–14945. [PubMed: 11279061]

Menzies FM, Cookson MR, Taylor RW, Turnbull DM, Chrzanowska-Lightowlers ZMA, Dong L, Figlewicz DA, Shaw PJ. Mitochondrial dysfunction in a cell culture model of familial amyotrophic lateral sclerosis. Brain. 2002; 125:1522–1533. [PubMed: 12077002]

Nikolaev A, McLaughlin T, O'Leary DD, Tessier-Lavigne M. APP binds DR6 to trigger axon pruning and neuron death via distinct caspases. Nature. 2009; 457:981–989. [PubMed: 19225519]

Pielage J, Fetter RD, Davis GW. Presynaptic spectrin is essential for synapse stabilization. Curr Biol. 2005; 15:918–928. [PubMed: 15916948]

Pielage J, Cheng L, Fetter RD, Carlton PM, Sedat JW, Davis GW. A presynaptic giant ankyrin stabilizes the NMJ through regulation of presynaptic microtubules and transsynaptic cell adhesion. Neuron. 2008; 58:195–209. [PubMed: 18439405]

Pielage J, Bulat V, Zuchero JB, Fetter RD, Davis GW. Hts/Adducin controls synaptic elaboration and elimination. Neuron. 2011; 69:1114–1131. [PubMed: 21435557]

Pilling AD, Horiuchi D, Lively CM, Saxton WM. Kinesin-1 and Dynein are the primary motors for fast transport of mitochondria in *Drosophila* motor axons. Mol Biol Cell. 2006; 17:2057–2068. [PubMed: 16467387]

Puls I, Jonnakuty C, LaMonte BH, Holzbaur EL, Tokito M, Mann E, Floeter MK, Bidus K, Drayna D, Oh SJ, et al. Mutant dynactin in motor neuron disease. Nat Genet. 2003; 33:455–456. [PubMed: 12627231]

Qin Y, Cheng C, Wang H, Shao X, Gao Y, Shen A. TNF-alpha as an autocrine mediator and its role in the activation of Schwann cells. Neurochem Res. 2008; 33:1077–1084. [PubMed: 18205044]

Reyes NA, Fisher JK, Austgen K, VandenBerg S, Huang EJ, Oakes SA. Blocking the mitochondrial apoptotic pathway preserves motor neuron viability and function in a mouse model of amyotrophic lateral sclerosis. J Clin Invest. 2010; 120:3673–3679. [PubMed: 20890041]

Richardson H, Kumar S. Death to flies: *Drosophila* as a model system to study programmed cell death. J Immunol Methods. 2002; 265:21–38. [PubMed: 12072176]

Russo GJ, Louie K, Wellington A, Macleod GT, Hu F, Panchumarthi S, Zinsmaier KE. *Drosophila* Miro is required for both anterograde and retrograde axonal mitochondrial transport. J Neurosci. 2009; 29:5443–5455. [PubMed: 19403812]

Schoenmann Z, Assa-Kunik E, Tiomny S, Minis A, Haklai-Topper L, Arama E, Yaron A. Axonal degeneration is regulated by the apoptotic machinery or a NAD+-sensitive pathway in insects and mammals. J Neurosci. 2010; 30:6375–6386. [PubMed: 20445064]

Sevrioukov EA, Burr J, Huang EW, Assi HH, Monserrate JP, Purves DC, Wu JN, Song EJ, Brachmann CB. *Drosophila* Bcl-2 proteins participate in stress-induced apoptosis, but are not required for normal development. Genesis. 2007; 45:184–193. [PubMed: 17417787]

Shah SB, Nolan R, Davis E, Stokin GB, Niesman I, Canto I, Glabe C, Goldstein LS. Examination of potential mechanisms of amyloid-induced defects in neuronal transport. Neurobiol Dis. 2009; 36:11–25. [PubMed: 19497367]

Stork T, Engelen D, Krudewig A, Silies M, Bainton RJ, Klämbt C. Organization and function of the blood-brain barrier in *Drosophila*. J Neurosci. 2008; 28:587–597. [PubMed: 18199760]

Wang C, Youle RJ. The role of mitochondria in apoptosis. Annu Rev Genet. 2009; 43:95–118. [PubMed: 19659442]

Wang XJ, Cao Q, Liu X, Wang KT, Mi W, Zhang Y, Li LF, LeBlanc AC, Su XD. Crystal structures of human caspase 6 reveal a new mechanism for intramolecular cleavage and self-activation. EMBO Rep. 2010; 11:841–847. [PubMed: 20890311]

Weber U, Paricio N, Mlodzik M. Jun mediates Frizzled-induced R3/R4 cell fate distinction and planar polarity determination in the *Drosophila* eye. Development. 2000; 127:3619–3629. [PubMed: 10903185]

Xue L, Igaki T, Kuranaga E, Kanda H, Miura M, Xu T. Tumor suppressor CYLD regulates JNK-induced cell death in *Drosophila*. Dev Cell. 2007; 13:446–454. [PubMed: 17765686]

Yang CS, Thomenius MJ, Gan EC, Tang W, Freel CD, Merritt TJ, Nutt LK, Kornbluth S. Metabolic regulation of *Drosophila* apoptosis through inhibitory phosphorylation of Dronc. EMBO J. 2010; 29:3196–3207. [PubMed: 20700104]
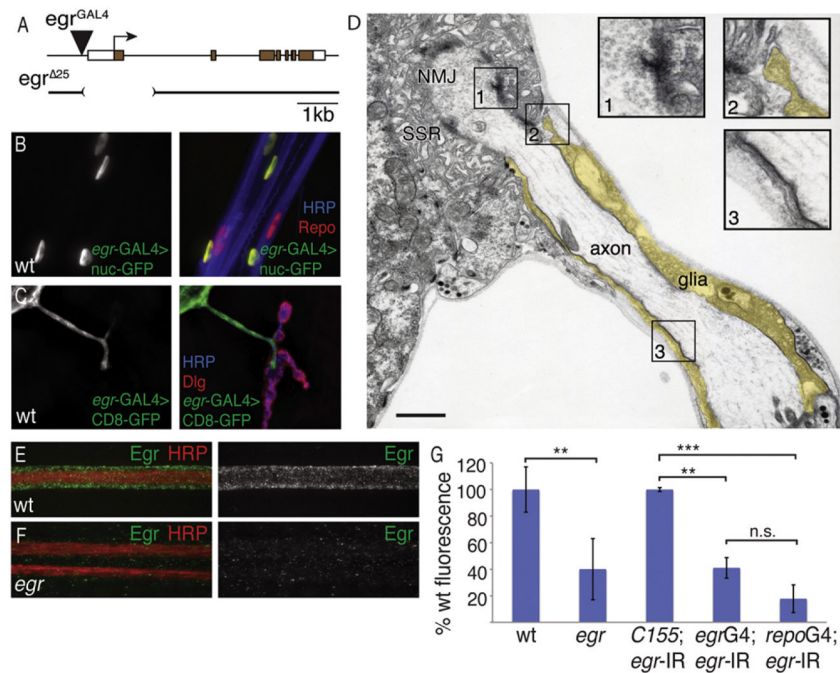
Figure 1. Eiger Is Present in a Subset of Peripheral Glia that Reside in Close Proximity to Motoneurons

(A) Schematic of the *eiger* locus. The *egr*-GAL4 insertion resides 21 bp upstream of the *egr* transcriptional start site.

(B) Motoneurons expressing nuclear-GFP (green, shown in isolation at left) driven in a subset of peripheral glia by *egr*-GAL4 and stained with Repo (red) to visualize all glia nuclei and HRP (blue) to visualize neuronal membranes.

(C) Expression of membrane-tethered GFP (CD8-GFP) driven by *egr*-GAL4 and visualized at the muscle 4 NMJ (shown in isolation at left, green in merged image at right). The presynaptic motoneuron membrane is stained with HRP (blue), and the postsynaptic SSR marker Dlg (red) delineates postsynaptic densities.

(D) Electron micrograph of an individual motoneuron axon, ensheathed by glia (pseudo-colored yellow), extending toward and contacting muscle 12 with a terminal NMJ surrounded by postsynaptic SSR. Insets (1–3) show magnified boxed regions as indicated. Inset 1 shows an active zone with accumulation of synaptic vesicles, inset 2 shows glial extension and contact with the muscle, and inset 3 shows characteristic septate junctions between glia and neurons. Scale bar, 500 nm.

(E) A projection image from confocal image stacks of an individual wild-type larval nerve. Eiger protein (green) localizes to glia that surround and ensheath the neurons (red).

(F) Two larval nerves from the *egr*$^{\Delta 25}$ mutant stained with the neuronal membrane marker HRP (red) showing loss of Eiger staining (green).

(G) Levels of Eiger immunoreactivity are quantified in nerves. wt = w^{1118} (ten animals); *egr* = *eiger*$^{\Delta 25}$/*eiger* $^{\Delta 25}$ (ten animals); C155; *egr*-IR = *elav*^{C155}-GAL4; *pUAS-egr*RNAi (four animals); *egr*G4; *egr*-IR = *egr*-GAL4; *pUAS-egr*RNAi (five animals); *repo*G4; *egr*-IR = *Repo*-GAL4; *pUAS-egr*RNAi (five animals). Error bars represent SEM. p values were determined using one-way ANOVA with post hoc Tukey-Kramer: **p < 0.01; ***p < 0.001. Statistical differences remain when comparisons are made using Student's t test. n.s., not significant.
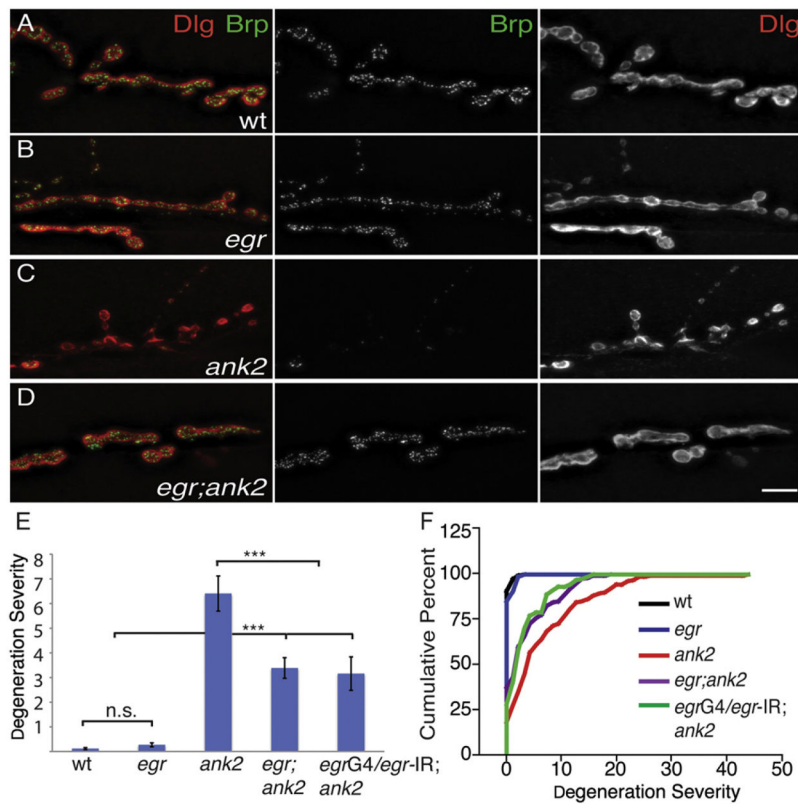
Figure 2. *eiger* Suppresses *ank2*-Dependent Degeneration at the NMJ

(A–D) Representative images of third-instar muscle 6/7 NMJs stained with the presynaptic active zone marker Brp (green, middle panels) and the postsynaptic marker Dlg (red, right panels). (A) A wild-type NMJ showing presynaptic Brp (green, middle panel) in perfect apposition with postsynaptic Dlg (red, right panel). (B) *eiger* null mutations do not affect NMJ morphology or colocalization of Brp (green, middle panel) and Dlg (red, right panel) at muscle 6/7. (C) NMJ of a homozygous *ank2* animal showing organized postsynaptic Dlg (red, right panel) with very little opposing presynaptic Brp staining, indicating that the presynaptic nerve terminal has been eliminated. (D) Animals that are homozygous for both *eiger* and *ank2* have a remarkably improved NMJ despite the presence of the *ank2* mutation. Presynaptic Brp (green, middle panel) now colocalizes with postsynaptic Dlg (red, right panel) staining. Scale bar, 10 μm.

(E and F) Quantification of degeneration severity (E) is measured as the average number of boutons retracted per individual NMJ, and cumulative percentage of degeneration severity (F) is plotted as cumulative frequency histogram for each genotype. wt = w^{1118} (n = 129 NMJs); *egr* = $egr^{\Delta25}/egr^{\Delta25}$ (n = 75 NMJs); *ank2* = $ank2^{2001}/ank2^{2001}$ (n = 141 NMJs); *egr; ank2* = $egr^{\Delta25}/egr^{\Delta25}$; $ank2^{2001}/ank2^{2001}$ (n = 129 NMJs); *egr*G4/*egr*-IR*; ank = egr*-GAL4/ *pUAS-egr*-RNAi; *ank/ank* (n = 90). Error bars represent SEM. p values were determined using one-way ANOVA with post hoc Tukey-Kramer: ***p < 0.001. Statistical differences remain when comparisons are made using Student's t test. n.s., not significant.
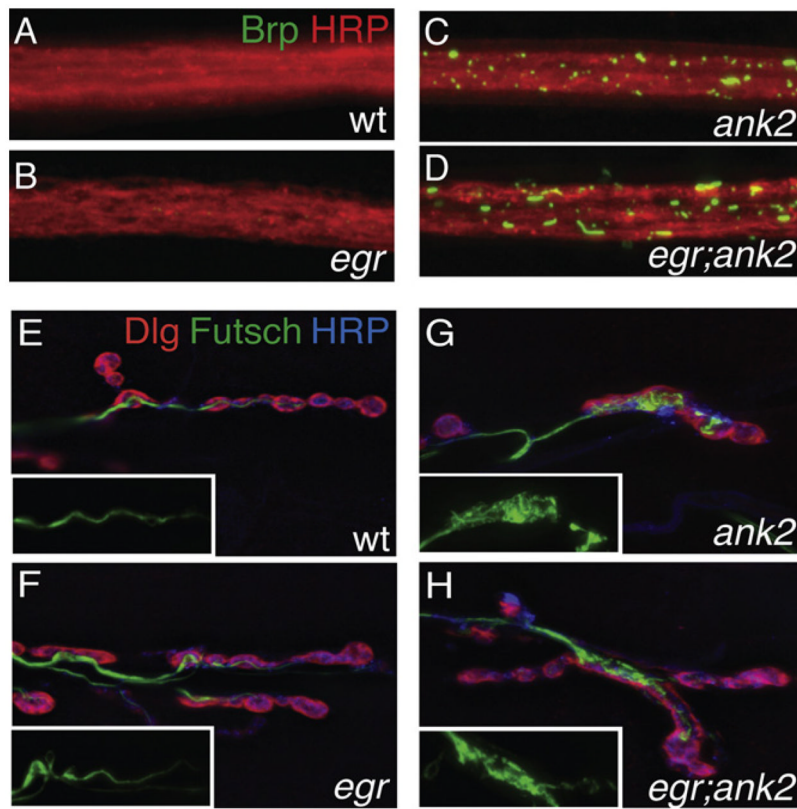
Figure 3. *eiger* Suppresses *ank2*-Dependent Degeneration Despite Persistent Cellular Stresses
(A–D) Representative images of individual third-instar nerve bundles stained for the neuronal membrane marker HRP (red) and the active zone marker Brp (green), which accumulates in *ank2* mutant axons. All images were taken at the same time with the same exposure conditions. (A) Wild-type nerve bundle with no visible Brp accumulations. (B) *egr* mutant nerve bundle that looks similar to wild-type with no visible Brp accumulations. (C) *ank2* nerve bundle showing significant amounts of Brp accumulations. (D) Nerve bundle from a double homozygous mutant for both *egr* and *ank2*, showing significant axonal Brp accumulations. Total Brp fluorescence intensity integrated over total nerve area is the following: wt = w^{1118} (n = 17 nerve bundles; average 8.16 arbitrary units); *egr* = $egr^{\Delta25}/egr^{\Delta25}$ (n = 17 nerve bundles; average 10.54 arbitrary units); *ank2* = $ank2^{2001}/ank2^{2001}$ (n = 21 nerve bundles; average 30.6 arbitrary units); *egr; ank2* = $egr^{\Delta25}/egr^{\Delta25}$; $ank2^{2001}/ank2^{2001}$ (n = 17 nerve bundles; average 31.6 arbitrary units). *ank2* and *egr; ank2* both have significantly more Brp total fluo-rescence than either wild-type or *egr* mutants alone ($p < 0.001$). The p values were determined using one-way ANOVA with post hoc Tukey-Kramer. Statistical differences remain when comparisons are made using Student's t test.
(E–H) Representative images of third-instar muscle 6/7 NMJs stained for the neuronal microtubule-associated protein Futsch (green), the presynaptic membrane marker HRP (blue), and the postsynaptic marker Dlg (red). Insets show Futsch staining only. (E) A wild-type NMJ shows an elongated and organized Futsch-positive microtubule cytoskeleton. (F) An NMJ lacking Eiger protein ($egr^{\Delta25}$) also shows an elongated and organized Futsch-positive microtubule cytoskeleton. (G) An NMJ mutant for *ank2* shows disorganized Futsch staining with accumulations within boutons. (H) Animals that are mutant for both *egr* and *ank2* do not restore microtubule organization.
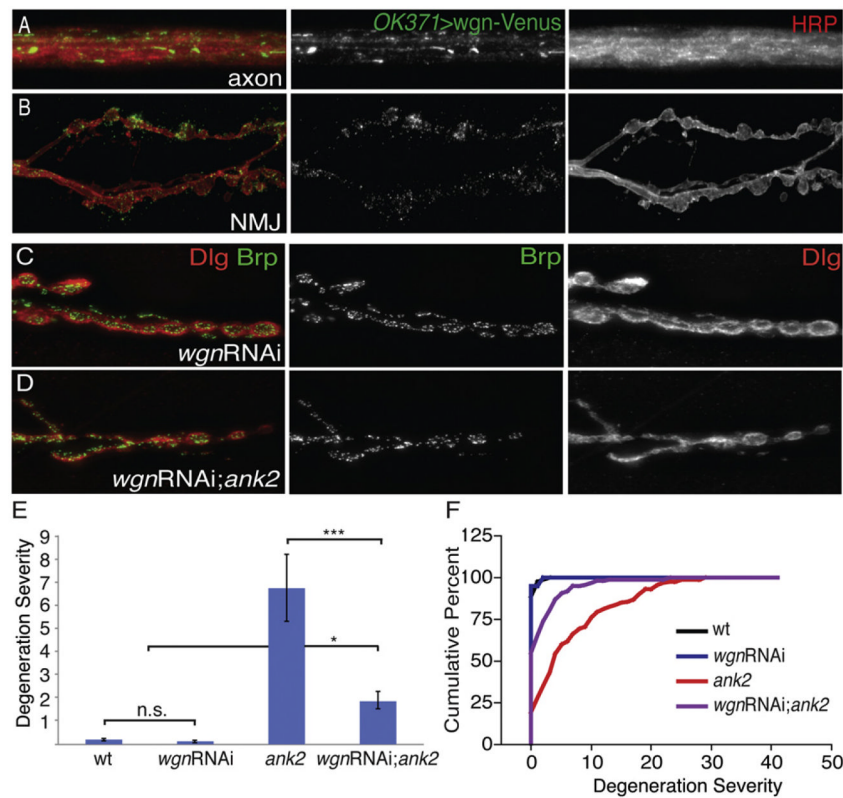
Figure 4. Presynaptic Knockdown of Wengen Suppresses *ank2*-Dependent Degeneration
(A) Wengen-Venus (green) expressed in motor neurons using *OK371*-GAL4 shows localization to motoneuron axons that are costained with the neuronal membrane marker HRP (red).
(B) Wengen-Venus (green) driven by *OK371*-GAL4. Wengen-Venus localizes to the NMJ, albeit at lower levels than in the axons.
(C) Neuronal-specific Wengen knockdown stained with the presynaptic active zone marker Brp (green) and the postsynaptic marker Dlg (red) at NMJ 6/7. Presynaptic expression of *wengen*-RNAi does not cause any significant synaptic degeneration.
(D) Representative image stained with Brp (green) and Dlg (red) showing suppression of *ank2*-dependent degeneration by neuronal expression of *wengen*-RNAi.
(E and F) Quantification of degeneration severity as in Figures 2E and 2F. wt = w^{1118} (n = 59 NMJs); *wgn*RNAi = *elav*^{C155}-GAL4/+; *wgn*RNAi/+; *ank2*^{2001}/+ (n = 58 NMJs); *ank2* = *ank2*^{2001}/*ank2*^{2001} (n = 52 NMJs); *wgn*RNAi; *ank2* = *elav*^{C155}-GAL4/+; *wgn*RNAi/+; *ank2*^{2001}/*ank2*^{2001} (n = 159 NMJs). *ank2* mutants have significantly more synaptic degeneration than either wild-type or *wengen*-RNAi larva ($p < 0.001$), whereas *wgn*-RNAi; *ank2* larva have significant suppression of *ank2*-dependent degeneration ($p < 0.001$). Error bars represent SEM. p values were determined using one-way ANOVA with post hoc Tukey-Kramer: *$p < 0.05$; ***$p < 0.001$. Statistical differences remain when comparisons are made using Student's t test. n.s., not significant.
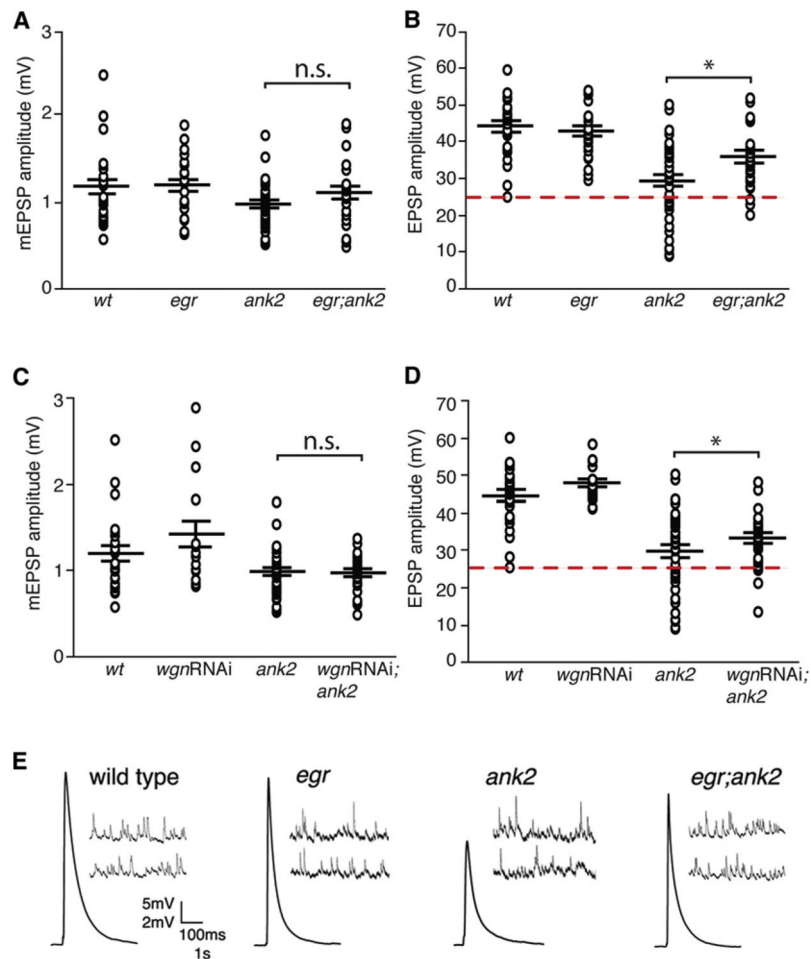
Figure 5. Synaptic Transmission Deficiencies in *ank2* Mutants Are Suppressed by Both *eiger* Mutations and *wengen*-RNAi

(A) Average mEPSP amplitude for wild-type, *egr*, *ank2*, and the double mutant *egr; ank2*. In (A)–(D), values are averages from individual recordings, and genotypic averages are shown as large horizontal bars with SEM indicated by the position of smaller horizontal bars above and below the mean. wt = w^{1118} (average mEPSP, 1.23 mV, n = 26); *egr* = eiger$^{\Delta 25}$/ eiger $^{\Delta 25}$ (average mEPSP, 1.2 mV, n = 24); *ank2* = ank2^{2001}/ank2^{2001} (average mEPSP, 0.98 mV, n = 40); *egr; ank2* = eiger $^{\Delta 25}$/eiger $^{\Delta 25}$; ank2^{2001}/ank2^{2001} (average mEPSP, 1.13 mV, n = 28). There is no significant difference between genotypes.

(B) The *ank2* mutants have a large number of recordings with average EPSPs below 25 mV, the limit of the wild-type distribution (red dash line). wt = w^{1118} (average EPSP, 44.2 mV, n = 26); *egr* = egr$^{\Delta 25}$/egr$^{\Delta 25}$ (average EPSP, 42.8mV, n = 24); *ank2* = ank2^{2001}/ank2^{2001} (average EPSP, 29.5mV, n = 40); *egr; ank2* = egr$^{\Delta 25}$/egr$^{\Delta 25}$; ank2^{2001}/ank2^{2001} (average EPSP, 35.9 mV, n = 28). A significant increase in EPSP amplitude is observed comparing *ank2* with *egr; ank2* (*p = 0.02, Student's t test).

(C) Average mEPSP amplitude for wild-type, *wgn*-RNAi, *ank2*, and *wgn*-RNAi; *ank2* larva. wt = w^{1118} (average mEPSP, 1.23 mV, n = 26); *wgn*RNAi = elav^{C155}-GAL4; *wgn*-RNAi (average mEPSP, 1.41 mV, n = 16); *ank2* = ank2^{2001}/ank2^{2001} (average mEPSP, 0.98 mV, n = 40); *wgn*RNAi; *ank2* = elav^{C155}-GAL4; *wgn*-RNAi/+; *ank2/ank2* (average mEPSP, 0.96 mV, n = 30). There is no difference comparing *ank2* with *wgn*-RNAi/+; *ank2/ank2*. n.s., not significant.

(D) Average EPSP amplitude for wild-type, *wgn*-RNAi, *ank2*, and *wgn*-RNAi; *ank2* larva. wt = w^{1118} (average EPSP, 44.2 mV, n = 26); *wgn*RNAi = *elav*^{C155}-GAL4; *wgn*-RNAi (average EPSP, 48.08 mV, n = 16); *ank2* = *ank2*^{2001}/*ank2*^{2001} (average EPSP, 29.5 mV, n = 40); *wgn*RNAi; *ank2* = *elav*^{C155}-GAL4; *wgn*-RNAi/+; *ank2/ank2* (average EPSP, 32.8 mV, n = 30). There is a significant increase in average EPSP amplitude comparing *ank2* and *wgn*RNAi; *ank2* (*p = 0.05, Student's t test).

(E) Representative EPSP and mEPSP traces for wild-type, *eiger*, *ank2*, and *egr; ank2*.
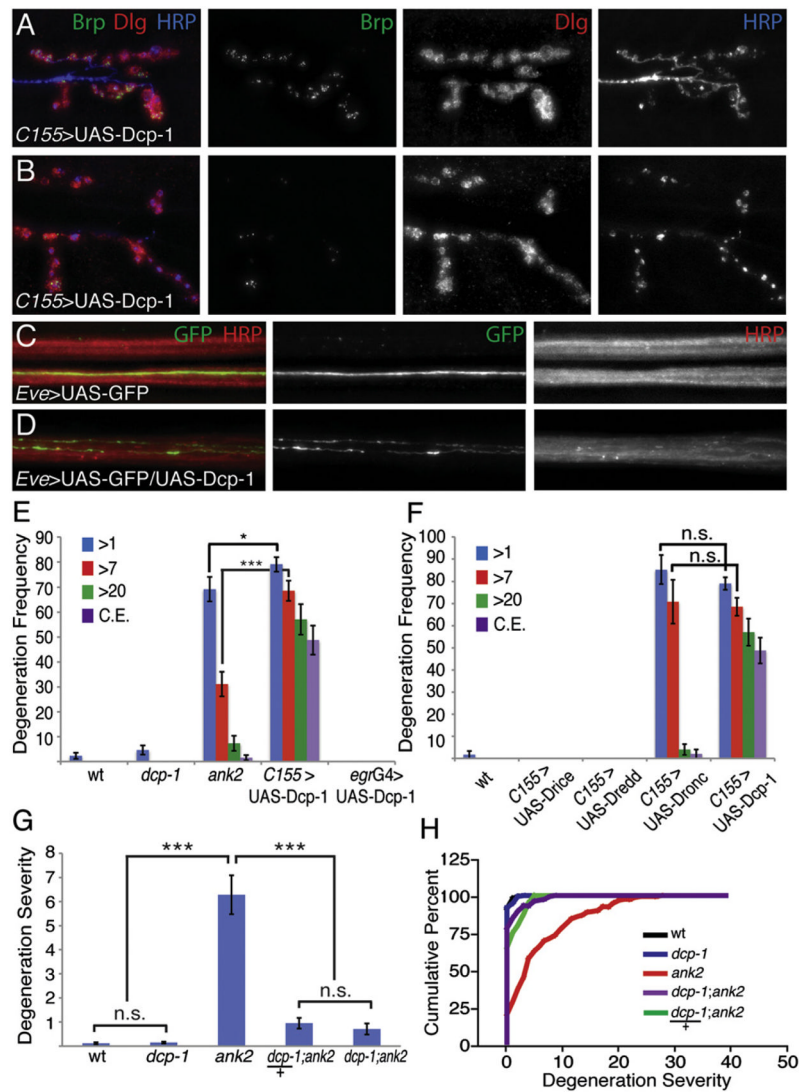
Figure 6. Dcp-1 Is Necessary and Sufficient for Prodegenerative Signaling

(A and B) Representative immunofluorescence images of NMJs at muscle 6/7 in larva expressing full-length Dcp-1 in neurons. NMJs are stained with the presynaptic marker Brp (green), the postsynaptic marker Dlg (red), and the neuronal membrane marker HRP (blue). A range of phenotypes exists when Dcp-1 is expressed in neurons, including significant synaptic degeneration (A) and complete presynaptic degeneration resulting in discontinuous HRP staining (B).

(C) Membrane-bound GFP expression (green) in single motoneurons being driven by the *EveRRa*-GAL4 driver within an otherwise wild-type nerve bundle. A single axon is visualized.

(D) Expression of full-length Dcp-1 and membrane-bound GFP (green) in single motoneurons by the *EveRRa*-GAL4 driver within a nerve bundle. Expression of Dcp-1 causes motoneurons to degenerate along their length.

(E) Quantification of degeneration frequency as measured by the average percentage of NMJs retracted per animal in wild-type, *dcp-1* homozygous mutants, *ank2*, and in larva expressing Dcp-1 in all neurons or in a subset of peripheral glia with *egr*-GAL4. wt = w^{1118} (n = 129 NMJs); *dcp-1* = *dcp-1^{Prev1}*/*dcp-1^{Prev1}* (n = 130 NMJs); *ank2* = *ank2^{2001}*/*ank2^{2001}*

(n = 122 NMJs); *C155 > UAS-Dcp1 = elav^{C155}-GAL4; UAS-Dcp-1/+* (n = 96 NMJs); *egr*G4 *> UAS-Dcp-1 = egr-GAL4/UAS-Dcp-1* (n = 80). Dcp-1 expression in neurons causes significantly more synaptic degeneration events that have >1 bouton, >7 boutons retracted, >20 boutons retracted, and complete synaptic eliminations (*p < 0.05; ***p < 0.001). Expression of Dcp-1 in Eiger expressing peripheral glia causes no degeneration.

(F) Quantification of degeneration frequency as measured above in wild-type and neuronal overexpression of Drice, Dredd, Dronc, or Dcp-1. wt = w^{1118} (n = 59 NMJs); *elav^{C155}-*GAL4; *UAS-Drice* (n = 100 NMJs); *elav^{C155}-*GAL4; *UAS-Dredd* (n = 40 NMJs); *elav^{C155}-*GAL4; *UAS-Dronc* (n = 50 NMJs); *elav^{C155}-UAS-Dcp-1* (n = 106 NMJs). Only expression of Dronc and Dcp-1 causes significantly more synaptic degeneration than in wild-type (p < 0.001). Note that data for *C155*-dependent *UAS-Dcp-1* are the same data as are presented in (E), reproduced to highlight specific comparisons.

(G and H) Quantification of degeneration severity as in Figures 2E and 2F. wt = w^{1118} (n = 129 NMJs); *dcp-1 = dcp-1^{Prev1}/dcp-1^{Prev1}* (n = 130 NMJs); *ank2 = ank2^{2001}/ank2^{2001}* (n = 122 NMJs); *dcp-1/+; ank2/ank2 = dcp-1^{Prev1}/+; ank2^{2001}/ank2^{2001}* (n = 40 NMJs); *dcp-1/ dcp-1; ank2/ank2 = dcp-1^{Prev1}/dcp-1^{Prev1}; ank2^{2001}/ank2^{2001}* (n = 127 NMJs). Mutant *dcp-1* as either a heterozygote or a homozygote significantly reduces the number of *ank2*-dependent synaptic degeneration events (p < 0.001). Error bars represent SEM. p values were determined using one-way ANOVA with post hoc Tukey-Kramer: ***p < 0.001. Statistical differences remain when comparisons are made using Student's t test. n.s., not significant.
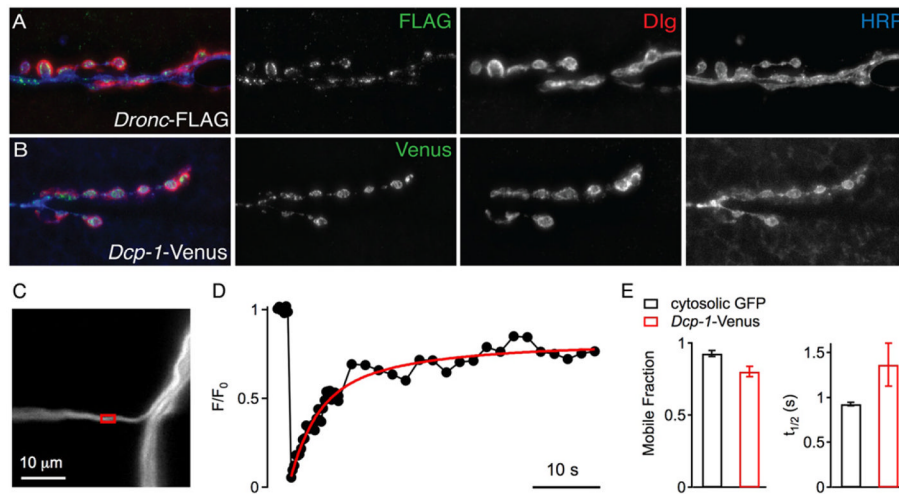
Figure 7. Caspases Localize to *Drosophila* NMJ

(A) Representative image of third-instar muscle 6/7 NMJs expressing FLAG-tagged initiator caspase, *Dronc*, in neurons. *Dronc*-FLAG (green) localizes within neurons demarcated by HRP (blue) and to boutons, Dlg (red). *Dronc*-FLAG, $elav^{C155}$-GAL4;; *pUAS-Dronc*-FLAG.

(B) Representative images of third-instar 6/7 NMJs expressing *Dcp-1*-Venus. *Dcp-1*-Venus, $elav^{C155}$-GAL4; *pUAS-Dcp-1*-Venus.

(C) Confocal image of an axonal segment of a motoneuron projecting to muscle 4 (segment A2), in which *UAS-Dcp-1*-Venus is expressed under the control of $elav^{C155}$. The red box marks the region that was bleached during the FRAP recording shown in (D).

(D) Normalized axonal FRAP time course. Fluorescence recovery was fitted with a double exponential function. Note that the *Dcp-1*-Venus fluorescence after the bleach pulse returns to ~75% of baseline fluorescence levels indicating that most of the *Dcp-1*-Venus is mobile within the axonal cytosol.

(E) Average mobile fraction (left) and half-maximum recovery time ($t_{1/2}$, right) of FRAP time courses recorded in axons expressing *Dcp-1*-Venus (n = 8, red), or cytosolic GFP (*OK371*-GAL4; UAS-*T2*-GFP, n = 6, black). The average mobile fraction of *Dcp-1*-Venus (0.81 ± 0.04) was slightly smaller than cytosolic GFP (0.93 ± 0.02; p = 0.03), and the average recovery of *Dcp-1*-Venus ($t_{1/2} = 1.36 \pm 0.24$ s) was slightly slower than in cytosolic GFP ($t_{1/2} = 0.93 \pm 0.02$ s; p = 0.05).
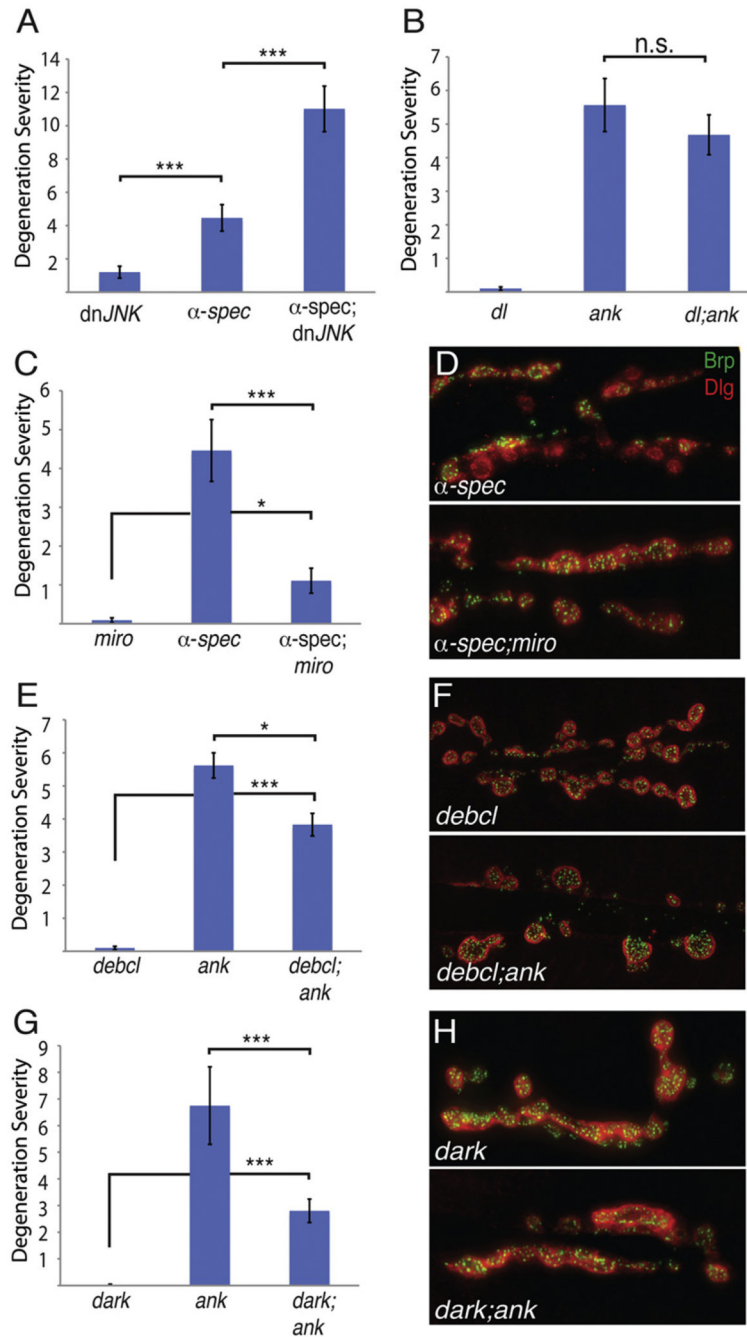
Figure 8. Mitochondria Are Required Locally for Axonal and Synapse Degeneration

(A and B) Mutations in either the *Drosophila* JNK homolog *bsk* or in the NFκβ homolog *dorsal* do not suppress synaptic degeneration caused by a disrupted spectrin/ankyrin skeleton. dnJNK = $elav^{C155}$-GAL4; dn*bsk* (n = 100 NMJs); *α-spec* = $elav^{C155}$-GAL4; *α-spec*-RNAi (n = 57 NMJs); *α-spec;* dn*JNK* = $elav^{C155}$-GAL4; *α-spec*-RNAi/+; dn*bsk*/+ (n = 106 NMJs); *dl* = dl^1/dl^1 (n = 100 NMJs); *ank2* = $ank2^{2001}/ank2^{2001}$ (n = 75 NMJs); dl^1; *ank2* = dl^1/dl^1; $ank2^{2001}/ank2^{2001}$ (n = 77 NMJs).

(C) Mutations in *miro* suppress the synaptic degeneration caused by neuronally expressed *α-spectrin*-RNAi (p < 0.001). *miro* = $elav^{C155}$-GAL4; *miro*^B682^/*miro*^B682^ (n = 88 NMJs); *α-*

spec = elav^{C155}-GAL4; *α-spectrin*-RNAi (n = 58 NMJs); *α-spec; miro* = elav^{C155}-GAL4; *α-spectrin*-RNAi/+; *miro* ^{B682}*/miro* ^{B682} (n = 209 NMJs).

(D) Representative images of third-instar muscle 6/7 NMJs stained with the presynaptic active zone marker Brp (green) and the postsynaptic marker Dlg (red). Neuronally expressed α-spectrin RNAi causes neuronal degeneration (top panel) and this is suppressed by the *miro* mutation (bottom panel).

(E–H) Mutations in known components of mitochondrial-dependent caspase signaling suppress *ankyrin*-dependent synaptic degeneration. (E) Mutations in *debcl* suppress *ankyrin*-dependent degeneration. *debcl = debcl*$^{[E26]}$*/debcl*$^{[E26]}$ (n = 60); *ank2 = ank2^{2001}/ank2^{2001}* (n = 151); *decbl; ank = debcl*$^{[E26]}$*/debcl*$^{[E26]}$; *ank2^{2001}/ank2^{2001}*(n = 103). (F) Representative images stained with presynaptic Brp (green) and postsynaptic Dlg (red). *debcl* mutant animal NMJs do not have any noticeable morphological abnormalities or synaptic degeneration (top panel); however, there is a significant suppression of *ankyrin*-dependent degeneration (bottom panel). (G) Mutations in *dark* suppress *ankyrin2*-dependent degeneration. *dark = dark^{CD4}/dark ^{CD4}* (n = 80); *ank2 = ank2^{2001}/ank2^{2001}* (n = 60); *dark; ank = dark^{CD4}/dark ^{CD4}*; *ank2^{2001}/ank2^{2001}* (n = 160). (H) Representative images stained with presynaptic Brp (green) and postsynaptic Dlg (red). Animals mutant for *dark* that produce NMJs do not have any noticeable morphological abnormalities or synaptic degeneration (top panel); however, there is a significant suppression of *ankyrin*-dependent degeneration (bottom panel). Degeneration severity is measured as above.

Error bars represent SEM. p values were determined using one-way ANOVA with post hoc Tukey-Kramer: *$p < 0.05$; ***$p < 0.001$. Statistical differences remain when comparisons are made using Student's t test. n.s., not significant.
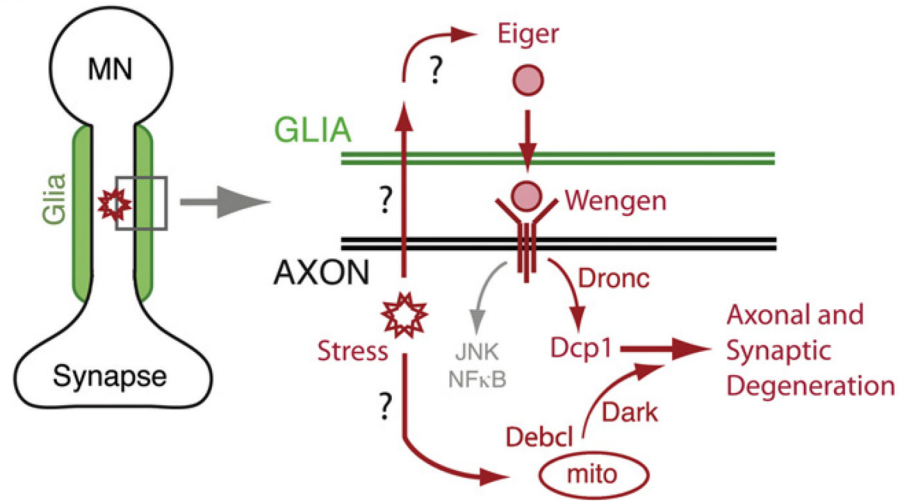
Figure 9. Summary and Model

(A) Summary of genetic data in support of prodegenerative-signaling pathways. (1) The loss of either Eiger within peripheral glia or the loss of Wengen within motoneurons suppresses *ankyrin*-dependent neuromuscular degeneration (neuronal stress) at the *Drosophila* NMJ. Based on these data, we propose that Eiger and Wengen establish a glial-derived, prodegenerative-signaling system. (2) Expression of either the initiator caspase Dronc or the effector caspase Dcp-1 is sufficient to cause synaptic degeneration at the NMJ. Additionally, Dcp-1 is necessary for prodegenerative signaling. Based on these data, we propose the involvement of a caspase-signaling system that is activated following disruption of the spectrin/ankyrin skeleton. (3) Mitochondria-dependent signaling (mito) participates in the neurodegenerative-signaling system at the *Drosophila* NMJ. A mutation in *miro* (not shown), which depletes mito-chondria from motor axons and synapses, significantly suppresses degeneration. Additionally, mutations in two genes, *debcl* and *dark*, previously shown to function downstream of disrupted mitochondria in other systems, suppress degeneration. Therefore, we propose the involvement of a mitochondria-dependent signaling system in the degenerative response.

(B) Proposed model for glial-derived prodegenerative signaling in *Drosophila* motoneurons. According to this model, a neuronal stress such as disruption of the spectrin/ankyrin skeleton is detected by surrounding peripheral glia, which respond by release of Eiger (TNF-α). Eiger is detected by Wengen (TNFR) in motoneurons and may lead to downstream caspase activation followed by disassembly of the motor axon and/or synapse. We also propose involvement of a mitochondrial-dependent signaling system involving Debcl and Dark that may function to potentiate the prodegenerative caspase response. Notably, there

may be direct signaling from a site of axonal stress to activation of mitochondria-dependent degenerative signaling.